Available online at www.sciencedirect.com
SCIENCE DIRECT®
Journal of Sound and Vibration 271 (2004) 547–575
JOURNAL OF SOUND AND VIBRATION
www.elsevier.com/locate/jsvi

Rotating vibration behavior of the turbine blades with different groups of blades

Gwo-Chung Tsai*

Department of Mechanical Engineering, National I-Lan Institute of Technology, I-Lan, Taiwan, ROC

Received 26 April 2002; accepted 10 March 2003

Abstract

The rotating vibration behaviors of full cycle of 60 blades are studied in this report. The dynamic analysis of two different structures in one of which there are 10 groups of 6 blades and in the other 5 groups of 12 blades, is performed to investigate behavior deviation. In this research, the following jobs are considered: (1) collect the geometric dimensions and material properties of a single blade, (2) create the finite element model of a single blade, a group of 6 blades and 12 blades, and full cycle of 60 blades, (3) perform the vibration analyses of a single blade, a group of blades and a full circle of 60 blades, (4) perform the steady state stress analysis of the blade with different rotating speed; (5) get the Campbell diagram for the full circle of blades, and (6) make comparisons between a group of 6 blades and a group of 12 blades.

The conclusions from the analyses are the following: (1) the contact elements are applied to groups of 6 and 12 blades systems and the highest stresses are observed at the location of the first neck of the blade root. These results completely agree very well with in-site observations. (2) The big differences were present in the Campbell diagram: resonant frequencies are observed in the first vibration group for the full system comprising the group of 6 blades and resonant frequencies are not found in the first vibration group of the full blade system made of the group of 12 blades. (3) The dynamic behavior of the full blade system comprised of a group of 6 blades was found much different from that of the full blade system made is of a group of 12 blades. (4) Excellent agreements for the vibration frequencies and mode shapes of a single blade and a full circle of blades are obtained between the FEA results and experimental data.
© 2003 Elsevier Ltd. All rights reserved.

1. Introduction

Failures of blades of the turbine (see Fig. 1) are observed sometimes in power plants. The blade failure will shoot down the electricity plane and affect the power supply. Generally, stopping

*Corresponding author.
E-mail address: gctsai@ilantech.edu.tw (G.-C. Tsai).

0022-460X/03/$ - see front matter © 2003 Elsevier Ltd. All rights reserved.
doi:10.1016/S0022-460X(03)00280-3

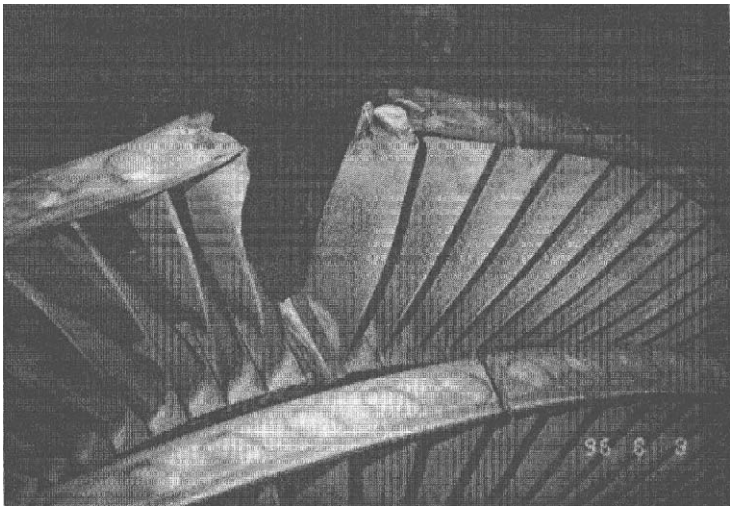

Fig. 1. The blade failure in the rotating blade.

supplying electricity causes economic loss for the power plant, because operation of the turbine engine has to be terminated and the cover of the engine has to be opened to check the turbine blade. Failure of blades may have different causes, such as the corrosion from the environmental pollution, deteriorated material properties, incorrect operation, resonant vibration, etc. In the dynamic analysis, the resonant vibration behavior can be analyzed and can be avoided based on the analytical results.

Generally, research on the turbine blades focus on vibration frequencies and mode shapes. For simplifying the analytical difficulties, a slender beam is used to replace the turbine blade. A single freestanding blade can be considered as a pre-twisted cantilever beam with an asymmetric aerofoil cross-section mounted at a stagger angle on a rotating disk. The starting solution for a simple stationary blade is obtained from the classical Euler–Bernoulli beam [1] with cantilever boundary conditions for bending vibration and non-circular rod for torsion vibration [1,2]. Coupled bending–torsion vibrations occur when the center of flexure does not coincide with the centroid as in the aerofoil blade cross-section and the vibrations are coupled between the two bending modes because of pre-twist. The problem becomes further complicated because of second order effects such as shear deflections, rotary inertia, fiber bending in torsion, warping of the cross-section, root fixing and Coriolis accelerations. In general the equations of motion will be six coupled partial differential equations coupled between the two bending deflections, the two shearing deflections, the torsion deflection and the longitudinal deflection. Further the warping function will be obtained by a modified Poisson equation, taking into account the dynamic conditions of the blade. Thus, theoretically it is an uphill task to determine the natural frequencies of an actual turbine blade with all the effects mentioned. Thus various researchers have derived solutions to the problem by considering individual aspects such as taper, pre-twist, asymmetry of cross-section centrifugal forces and making simplified assumptions with regard to second order effects. Broadly speaking, this work was carried through two different approaches, viz., continuous system and discrete modelling of the blade [3].

The continuum approach for a freestanding blade requires much analytical work before a numerical procedure can be adopted. Discretizing the blade and using appropriate element relations is simpler than the analytical work that goes with continuum methods and thus many researchers favor discrete methods. Other distinct advantages of discrete models are their compatibility to complicated problems like laced, shrouded and packeted blades, and the availability of well-tested finite element programs to model any complicated blade group. The discrete analysis techniques can be broadly classified into the following methods as applied to turbine blade problems: (1) Holzer's method [4], (2) The Myklestad/Prohl method [5], (3) matrix methods [6], (4) finite difference method [7–9], and (5) finite element method [10,11]. The finite element method [10] has become popular in many research fields. Dokumaci [10] used the matrix displacement method to determine natural frequencies of pre-twisted tapered blades. The matrix displacement method was extended to determine coupled bending–bending–torsion vibration characteristics of a rotating blade. Later the finite element method was applied to study the coupled bending–bending–torsion vibration modes taking into account the effect of root flexibility. Murthy and Murthy [12] developed a finite element formulation of rotating pre-twisted tapered beams with five degrees of freedom for each element. Gupta and Rao [13] extended tapered twisted elements to Timoshenko beam elements. Abbas [14] developed simple finite elements for thick pre-twisted blades accounting for shear and rotary inertia; Putter and Manor [15] included the effect of tip mass and also presented a high precision rotating beam element based on the fifth-degree polynomial. Singh and Rawtani [16] solved the classical wave equation for torsion vibration of a blade including root stiffness at the fixed boundary. Nagaraj considered the effect of attachment flexibility and Sahu [17] determined the torsion vibrations of pre-twisted rotating blades by finite element method based on Rayleigh–Ritz and Galerkin procedures. The finite element method was extended to determine the natural frequencies of packeted blades in coupled bending–bending–torsion modes. Rieger and Nowak [18] have developed a three-dimensional (3D) finite element model of the blade root and wheel root that incorporates gap elements at the root interface. The so-called super element can be used to generate automatically the mesh for the remaining blades of a group so that natural frequencies and mode shapes can be determined. A finite element model of a group of blades with rectangular cross-section has been presented in the tangential mode [19]. Salama and Petyt [20] used the finite element method and periodic structural analysis for the tangential vibration of packeted blades; both the positions of the lacing wire and rotation were taken into account. Eight node iso-parametric solid elements were used by Sagendorph [21] to model a fan blade with a tie-wire. Calculations were made for free and for locked configurations. Comparison of the free shroud condition with experimental data gave agreement to within 10% for the first 10 modes. Holography was used to verify mode shapes, which compared favorably with the finite element method results. In [22], 2D and 3D finite element technologies were applied to investigate the cracking of the SSME HPFTP first and second stage turbine blades. The 2D model that was comprised of 3500 plane strain elements was used to perform a number of parametric studies in order to reduce the computer runs using the large 3D model. The loading on the models stems form spin, pressure, and thermal that corresponded to the full power level. Only one blade model was created and analyzed. A finite beam element for vibration analysis of a rotating tapered beam including shear deformations, and rotary inertia is proposed [23]. The finite element has four degrees of freedom, and accounts for linear tapering in two planes. Explicit expressions for the finite element mass and stiffness matrices

are derived using the consistent mass approach, while accounting for the centrifugal stiffness effects. The new element is applied to calculate the first 10 free vibration modes for both fired and hinged and conditions of rotating tapered Timoshenko beam. The finite element method is also applied to predict the life of a created disk attachment region for a low-pressure steam turbine stage operating in a wet steam environment [24]. The strategy is based on a 'drop-notch' approach to remove the existing stress corrosion cracking. In [24], the fracture mechanical concepts combined with the finite elements are used to predict the crack growth life. The drop-notch procedure is to remove the top hook of the disk attachment and machine new grooves on the existing rim. In 1994, Rand applied a Galerkin-type approach to investigate the free vibration behavior of thin walled blades made by the composite materials [25]. Shiau et al. [26] studied the vibration behavior of blades made by the composite laminate, and the orientation of layup was also considered. Liew et al. [27–31] developed an energy approach with the Ritz minimization procedure to arrive at a governing eigenvalue equation. The admissible pb-2 shape functions which comprise sets of mathematically complete 2D orthogonal polynominals and a basic function are introduced to account for the boundary constraints. The effects of angle of twist, thickness variation and geometric parameters on the vibration frequencies and modes are examined. These theories can get accurate results for the pre-twisted cantilever trapezoidal plate, unsymmetric laminate blade and composite shallow conical shells. Eight-node element for the laminated blade was presented in [32]. Effects of radius of the disk, aspect ratio and rotating speed on the system dynamic behaviors and/or the optimum design are studied. In their studies, they found most of the bending modes of rotating laminated blade could be significantly affected by the rotating speed and the radius of the disk. In Ref. [32], Lin applied the finite element method to investigate the non-linear hydro-elastic behavior of composite propellers. The formulation used displacements as unknowns in the structural part and the strength of the vortex as unknowns in the fluid part. A coupled matrix derived from the Bernoulli equation and hydrostatic pressure in terms of the strength of the vortex enforced compiling between the fluid and structure. Finite element method is applied to investigate the vibration behaviors of mistuned bladed diesel assemblies [33]. The modelling technique employs a component mode synthesis approach to systematically generate a reduced order model of the rotor. The approach makes it feasible to predict the forced response statistics of mistuned bladed disk using Monte Carlo simulations. The above developments can verify that the finite element method can perform many analyses in many fields and different structures. But the systematic dynamic analyses for the blade–disk assemblies are not found. In this paper, the modal analysis of a single blade, the dynamic behavior of a group of blades, and the vibration analysis of fan system of a circle of blades are carried out and finally the harmonic analysis for the system of blade–disk assembly were performed to investigate the stress distribution and find the safety factor of the system.

In this research, the geometric dimension of a single blade is measured by using 3D accuracy measurement system and combined with the mathematical equations to obtain the complicated and exact geometric data of the blade. Combination of the blade geometry with the dimensions of disk, the solid model of a single blade and full circle blade model can be generated. After creating the solid model of a single blade and full circle of blades, the finite element model can be created by using the mapped mesh method. After creating the blade model and a circle of blades, the model analysis for the blade system with different rotating speeds will be performed. Based on the modal analysis, the Campbell diagram of a circle of blade system will be plotted and the resonant

frequencies will be obtained. Next, the harmonic analysis will be performed to check the stress distribution as the modal frequencies met the resonant frequencies. The excellent agreements for the vibration frequencies and mode shapes of a single blade and a full circle of blades are obtained between the FEA results and experimental data.

2. Background of theory

Because of the nature of blade geometry and loading, structural analysis of the blade is possible only by means of numerical methods. The main advantage of the finite element method is generally applied to complicated blade geometry. The blade is fixed with the setting angle on the rotating rigid disk of radius. The Coriolis effects are neglected, but the damping effects, the effects of pre-twist, as well as taper, are considered. In addition, the external forces are calculated from the thermodynamics and functions of frequency only.

To analyze the dynamic behaviors of the blade system, a finite element method using eight node iso-parametric solid elements is applied. The displacement field $\vec{\mathbf{u}}$ which include the pre-vibration deformation in each element can be expressed in terms of nodal translation and rotational displacements (u_i, v_i, w_i) and $(\Phi_{xi}, \Phi_{yi}, \Phi_{zi})$, respectively. It can be expressed as

$$\vec{\mathbf{u}} = [D]\vec{\mathbf{q}}, \tag{1}$$

where the displacement field vector $\vec{\mathbf{u}} = [u, v, w]^{\mathrm{T}}$, the nodal displacement vector

$$\vec{\mathbf{q}} = [u_1, v_1, w_1, \Phi_{x1}, \Phi_{y1}, \Phi_{z1}, \ldots, u_9, v_9, w_9, \Phi_{x9}, \Phi_{y9}, \Phi_{z9}],$$

and $[D]$ is the displacement functions of position

$$\{\varepsilon\} = [B]\{q\}, \tag{2}$$

where the strains

$$\{\varepsilon\} = \{\varepsilon_x, \varepsilon_y, \varepsilon_z, \gamma_{xy}, \gamma_{yz}, \gamma_{zx}\}^{\mathrm{T}},$$

and $[B]$ are the strain functions of position.

The finite element equation for a geometrically non-linear 3-D solid element is written as

$$[M]\{\ddot{u}\} + ([k_D] + [k_L] + [k_G])\{u\} = \{F_{ext}\}, \tag{3}$$

in which $[k_D], [k_L]$ and $[k_G]$ are the linear stiffness matrix, initial displacement matrix, and geometric matrix, respectively, $\{F_{\mathrm{ext}}\}$ are the external forces, the matrices are defined as

$$[M] = \rho \int_{vol} [D]^{\mathrm{T}}[D]\,\mathrm{d}v, \tag{4}$$

$$[K_D] = \int_{vol} [B]^{\mathrm{T}}[D][B]\,\mathrm{d}v, \tag{5}$$

$$[K_L] = \int_{vol} ([B]^{\mathrm{T}}[D][B_L] + [B_L]^{\mathrm{T}}[D][B_L] + [B_L]^{\mathrm{T}}[D][B])\,\mathrm{d}v, \tag{6}$$

$$[K_G] = \int_{vol} [T]^{\mathrm{T}} \begin{bmatrix} \sigma_x & \tau_{xy} \\ \tau_{xy} & \sigma_y \end{bmatrix} [T] \, \mathrm{d}v. \tag{7}$$

In these equations, $[B]$ and $[B_L]$ are linear and non-linear strain–displacement transformation matrices, $[D]$ is the material property matrix, and $[T]$ is a matrix defined purely in terms of co-ordinates. The equation is formed on the basis of an updated Lagrangian description [34] and is solved according to the Newton–Raphson procedures [35].

The expression of the rotating blade includes rotational effects, i.e., the rotational stiffness matrix and the centrifugal load. The Lagrange equation and the kinetic energy of the rotating blade are derived [36]. The expression for the rotational stiffness matrix is

$$[k_R] = \rho \int_{vol} [G_s]^{\mathrm{T}} [A][G_s] \, \mathrm{d}v, \tag{8}$$

$$[A] = \begin{bmatrix} \boldsymbol{\Omega}_y^2 + \boldsymbol{\Omega}_z^2 & -\Omega_x\Omega_y & -\Omega_x\Omega_z \\ -\Omega_x\Omega_y & \boldsymbol{\Omega}_x^2 + \boldsymbol{\Omega}_z^2 & -\Omega_z\Omega_y \\ -\Omega_x\Omega_z & -\Omega_z\Omega_y & -\boldsymbol{\Omega}_x^2 + \boldsymbol{\Omega}_y^2 \end{bmatrix}. \tag{9}$$

In Eq. (8), $[G_s]$ is the displacement interpolation matrix, $[A]$ is the angular velocity matrix, and ρ is the density of the blade. The expression of the centrifugal load is

$$\{F_R\} = \rho \int_{vol} [G_s]^{\mathrm{T}} [A] \begin{Bmatrix} x \\ y \\ z \end{Bmatrix} \mathrm{d}v. \tag{10}$$

Then equations of motion for an element for the rotating blade subjected to a centrifugal force is obtained by combining the above equations

$$[M]_e\{\ddot{u}\} + ([K_D]_e + [K_L]_e + [K_G]_e - [K_R]_e)\{u\} = \{F_{ext}\}_e + \{F_R\}_e. \tag{11}$$

The equations of motion for the system of the rotating blade in global co-ordinate system can be obtained by assembling all the governing equations of each element as follows:

$$[M]_g\{\ddot{\delta}\} + [K]_g\{\delta\} = \{F\}_g, \tag{12}$$

where $\{\delta\}$ denotes the displacement vector including the total number of degree of freedom of the system.

3. Experimental procedure

The experimental set-up for measuring the natural frequencies and mode shapes of the blade–disk assemblies are plotted in Fig. 2. Ten Kistler acceleration meters are stocked on the blade–disk assemblies that the finite element model is generated. The MB 50 type 409 20Kgf shaker is used to excite the blade–disk assemblies. The Kistler acceleration meters will be connected to the Sig-Lab 20–42 FFT machine, the data recollected from the FFT machine, then MEscope software will be applied to perform the analysis to get the mode shapes and frequencies. The experimental results

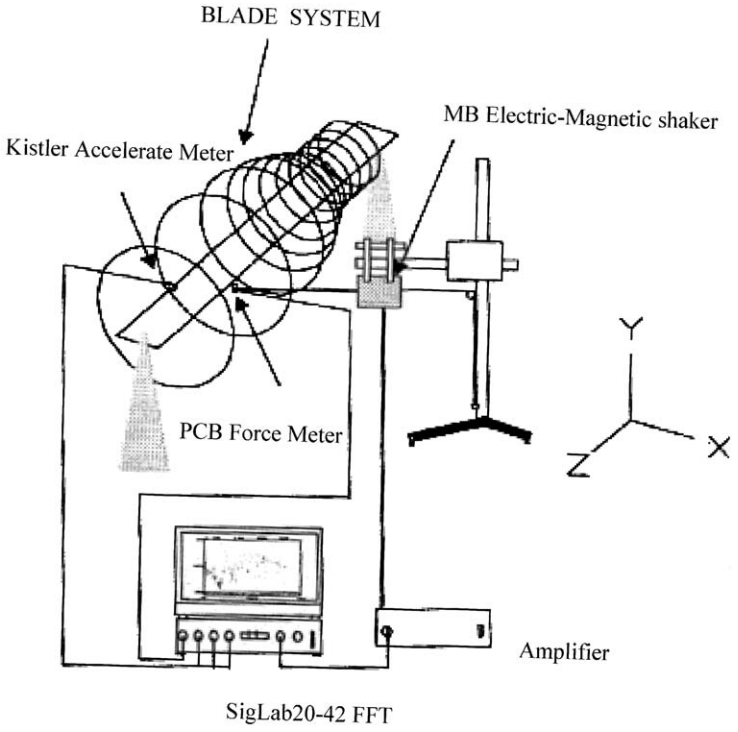

Fig. 2. Vibration equipment set-up.

will be used to compare with that obtained from the finite element analysis. Based on these comparisons, the results observed from the finite element analysis can be adjudged to be correct.

4. Modal analysis of a single blade

The finite element model of a single blade is plotted in Fig. 3. ANSYS [37] finite element package would be used to perform the finite element analysis. The element used in the model is Solid45 eight node structural element. In this single blade finite element, there were 322 elements and 641 nodes. The material properties of blade is listed in Table 1.

The free–free vibration of single blade is analyzed without any constraints and the results are shown in Table 2 and the mode shapes are plotted in Figs. 4–7.

Using hammer to strike and Mescope software to perform the free–free vibration experiments also obtain the test data. In Table 3 the comparison between the finite element results and the experimental data is shown.

The results obtained from finite element analysis agree very well with that of the experimental data. From these comparisons, the finite element model created in Fig. 1 can be used to investigate

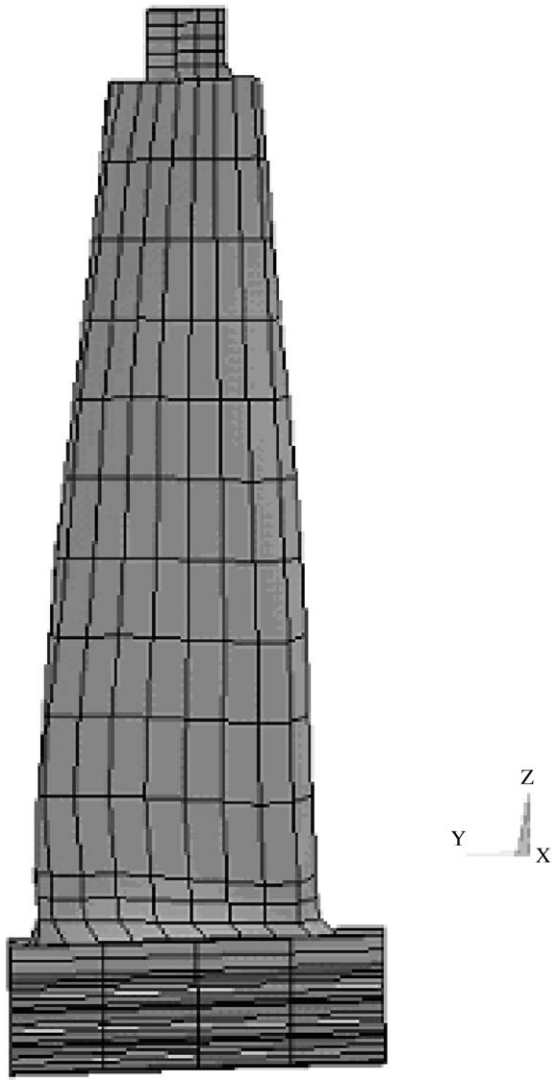

Fig. 3. Finite element model of a single blade without disk.

Table 1
Material properties of blade

Young's modulus	Poisson ratio	Density	σ_{yield}
2.127E8 kg mm/s^2/mm^2	0.27	7.77×10^{-6} kg/mm^3	6.66×10^5 kg mm/s^2/mm^2

the dynamic behavior of the real blade. The mass measured from the finite element model and weighted using the weight meter is listed in Table 4.

The deviation for both values is only 0.678%; therefore, the finite element model of the blade can be reliable to simulate the real blade behavior completely.

Table 2
Free–free vibration natural frequencies and modes

Mode	Frequencies (Hz)	Modes
1	766.1	Bend
2	1821.5	Twist
3	2243.7	Bend
4	3411.3	Bend + twist

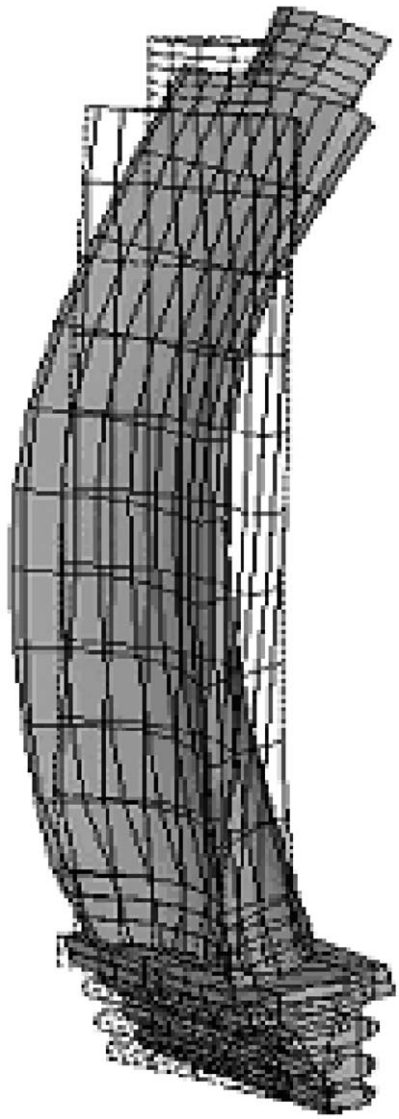

Fig. 4. Mode 1 of a single blade.

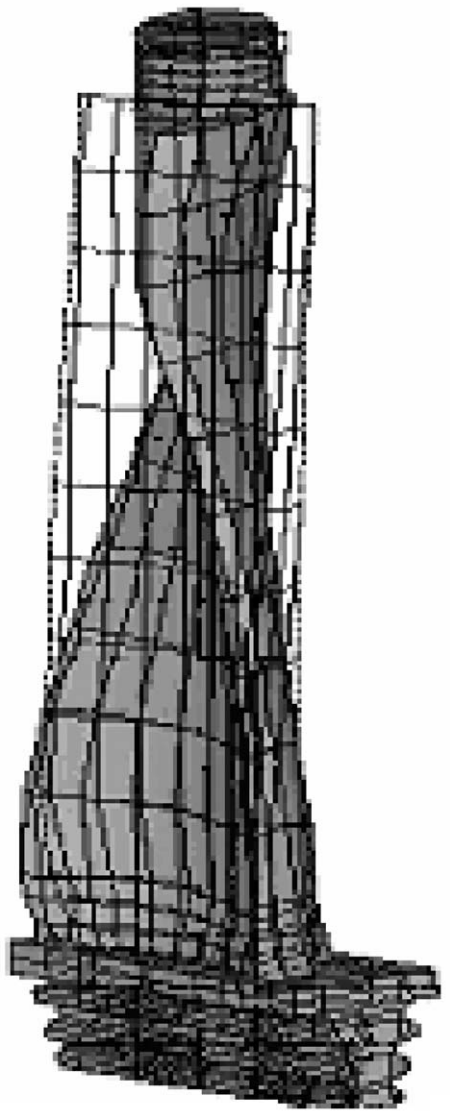

Fig. 5. Mode 2 of a single blade.

5. Rotating vibration analysis of a circle of 60 blades with different groups of blades

In this section, the finite element model of a circle of 60 blades comprised of 10 groups of blades (each group has 6 blades) and 5 groups of blades (each group has 12 blades) and the supported disk are created. For 10 groups of blades, it was shown in Fig. 8 that each group would have 6 blades. For 6 group of blades, it was shown in Fig. 9 that each group would have 12 blades.

It is hard to see from these finite element models to perceive their differences. It is because these differences exist only at the connection between the 6th blade and 7th blade in each group. For the

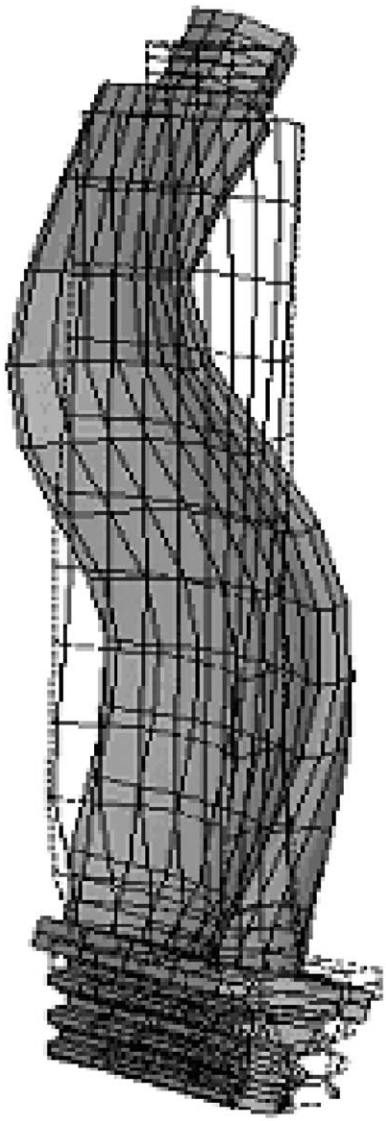

Fig. 6. Mode 3 of a single blade.

group of 6 blades it makes sure that there is no connection between the 6th blade and 7th blade. But for the group of 12 blades, complete connection exists at the location of the shroud of 6th blade and 7th blade. The other considerations are that material properties and boundary conditions remain the same. An important consideration with the bottom of the disk is that we must be sure that the locations of the fixed boundary conditions are at the connection surface between the disk and major shaft. If the fixed boundary conditions are not at the location of the connection surface between the disk and major shaft, one gets different nature frequencies and an erroneous Campbell diagram. Another key point for these models is that the contact element

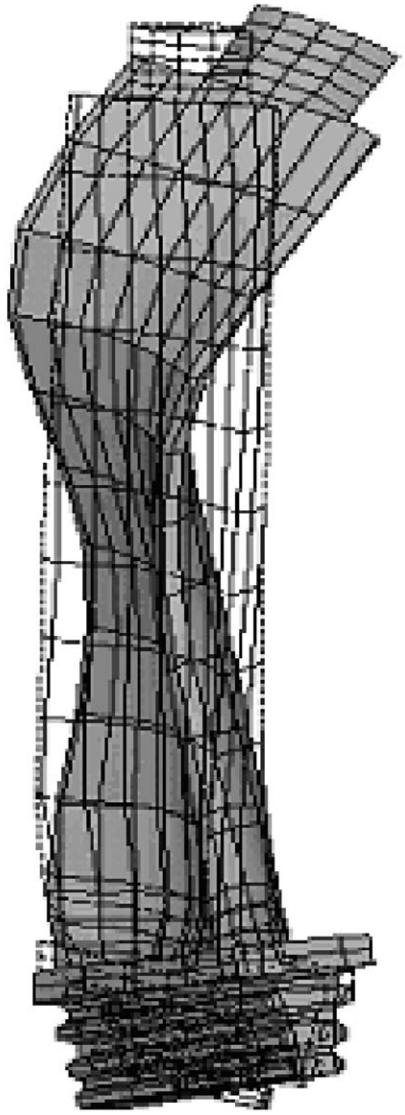

Fig. 7. Mode 4 of a single blade.

Table 3
Free–free vibration results

Mode	f (Hz) (experiment)	f (Hz) FEM	Error (%)
1	802.3	766.1	4.47
2	1823.1	1821.5	0.01
3	2212.4	2243.7	−1.43
4	3423.3	3411.3	0.03

Table 4
Mass comparison

Real measurement (g)	Calculation from FEM (g)	Error (%)
1043	1049.41	0.678

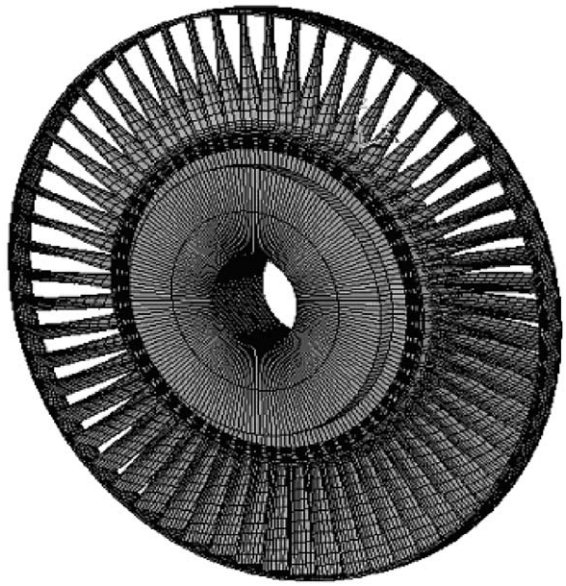

Fig. 8. The finite element model of full circle of 10 groups of 6 blades.

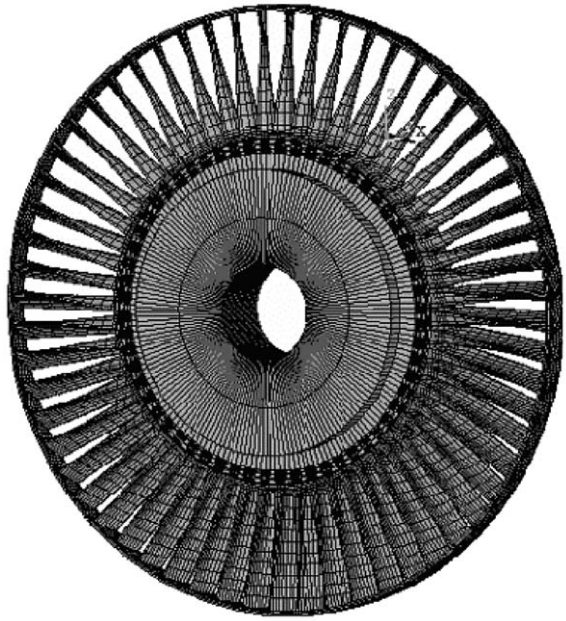

Fig. 9. The finite element model of full circle of 5 groups of 12 blades.

between the blade root and disk used in the static analysis must be deleted and the nodes between the blade roots and disk must be merged together to perform the dynamic analysis. And based on the static analysis, the blade root will rise up during the rotating motion and cause the top part of the neck of each blade root to contact the disk and the bottom part of the neck of each blade would depart away from the disk. Therefore, the merge of the nodes must be selected carefully to completely reflect the system's contact conditions.

The rotating speed of a circle of 60 blades is from 0 to 6000 r.p.m. For getting the accurate Campbell diagram, the dynamic analysis for full system of 60 blades must be performed with an increment of 500 r.p.m. The vibration results are shown in Table 5.

From these results, the first vibration group for a circle of blades comprised of a group of 6 blades has 10 modal shapes (frequencies from 331.9 to 336.20 Hz) and the range of frequencies is only about 5 Hz. The second vibration group will have 20 modal shapes and frequencies are from 699.70 to 806.66 Hz. The third vibration group can get 20 modal shapes. For a circle of 60 blades comprised of a group of 12 blades, their vibration modes and frequencies are summarized in the following. The first vibration group only has five modal shapes (frequencies from 339.53 to 343.98 Hz), the second vibration group can get 15 modal shapes (frequencies from 714.28 to 900.79 Hz), and the third vibration group can get 30 modal shapes. These results indicated that the first vibration group for a group of 6 blades has 6 five more modal shapes compared with that for a group of 12 blades. Also the modal shape of the 2nd vibration group and 3rd vibration group of a group of 12 blades are always less than those of the group of 6 blades. The differences between these two structures are not so many; their differences can also be shown in the Campbell diagram plotted in Figs. 10 and 11. In Fig. 10, the Campbell diagram for a group of 12 blades is plotted and that for a group of 6 blades is plotted in Fig. 11.

In Figs. 10 and 11, the straight line plotted from (0,0) point to the right of the vertical line on the top line represents the nth harmonics line. The almost horizontal straight line from left side to the right side is the frequencies line of the blade system as a function of rotating speed. The values of cross-points of the nth harmonics line with the vibration frequencies line are possible values of the resonant frequencies. But the possible resonant frequencies must be double checked with the nodal diameter from the mode shapes, and the nth harmonics line number must be coincident with the same nodal diameter. Then the frequencies at the cross-point are the exact resonant frequencies that the structure will get the higher amplitude of vibrations and may cause the catastrophic failure of blades. From these two Campbell diagrams, the range of the 1st frequency group for the group of 12 blades is smaller than that of the group of 6 blades. The range of the 2nd frequency group for the group of 12 blades is larger than that of the group of 6 blades. The range of the 3rd frequency group for the group of 12 blades is also larger than that of the group of 6 blades. The cross-point for the 1st group of both groups of blades are very closed from the Campbell diagram. The nodal diameter for both groups of blades is also listed in Table 5. The very interesting thing is that the system with the group of 6 blades has the nodal diameter number from 0 to 5 and the nodal diameter is only 0, 1 or 2 for the blade system with the group of 12 blades. The higher nodal diameters number (3, 4, and 5) appeared in the system with the group of 6 blades are not found in the first vibration group of the blade system comprised of the group of 12 blades. For completely distinguishing these differences, the vibration mode shape is shown in Figs. 12–15 for the system with a group of 6 blades. In Fig. 12, it is obvious that there is no any nodal diameter are shown in the figure and the concave shape is observed. The symbols A, B,…,I

Table 5
Vibration results of full circle of 10 and 5 groups blade

Vibration frequencies and nodal diameter				
Mode	5 groups of 12 blades		10 groups of 6 blades	
	Frequency (Hz)	Nodal diameter	Frequency (Hz)	Nodal diameter
(Mode 1–37)				
1	339.53	T1ND 0	337.09	T1ND 0
2	343.53	T1ND 1	340.96	T1ND 1
3	343.53	T1ND 1	340.96	T1ND 1
4	343.97	T1ND 2	341.16	T1ND 5
5	343.98	T1ND 2	341.20	T1ND 4
6	714.28	B2ND 1	341.20	T1ND 4
7	714.29	B2ND 1	341.32	T1ND 3
8	730.48	B2ND 0	341.32	T1ND 3
9	733.64	B2ND 2	341.43	T1ND 2
10	733.65	B2ND 2	341.43	T1ND 2
11	776.94	B2ND 3	709.88	B2ND 1
12	776.95	B2ND 3	709.88	B2ND 1
13	796.88	B2ND 4	724.17	B2ND 0
14	796.90	B2ND 4	729.92	B2ND 2
15	803.75	B2ND 5	729.93	B2ND 2
16	889.63	B2ND 5	769.09	B2ND 3
17	894.17	B2ND 6	769.11	B2ND 3
18	894.19	B2ND 6	783.83	B2ND 4
19	900.77	B2ND 7	783.85	B2ND 4
20	900.79	B2ND 7	787.73	B2ND 5
21	1318.11	T3ND 4	811.23	B2ND 5
22	1321.03	T3ND 4	811.92	B2ND 6
23	1321.12	T3ND 4	811.93	B2ND 6
24	1321.21	T3ND 5	813.33	B2ND 7
25	1321.21	T3ND 5	813.34	B2ND 7
26	1329.22	B3ND 5	814.69	
27	1369.93	B3ND 8	814.70	
28	1370.02	B3ND 8	816.27	
29	1375.11	B3ND 10	816.28	
30	1375.21	B3ND 10	817.19	
31	1382.82	B3ND 10	1301.01	
32	1387.03	B3ND 12	1341.02	
33	1387.12	B3ND 10	1341.02	
34	1390.14	B3ND 10	1344.71	
35	1390.23	B3ND 10	1344.71	
36	1397.21		1347.04	
37	1415.62		1347.04	
(Mode 38–74)				
38	1415.62		1347.33	
39	1416.04		1347.33	
40	1416.04		1347.33	
41	1417.81		1356.41	
42	1430.52		1370.62	

Table 5 (*continued*)

Vibration frequencies and nodal diameter				
Mode	5 groups of 12 blades		10 groups of 6 blades	
	Frequency (Hz)	Nodal diameter	Frequency (Hz)	Nodal diameter
43	1430.52		1370.74	
44	1433.04		1373.82	
45	1433.04		1373.82	
46	1433.12		1375.01	
47	1435.62		1375.13	
48	1435.62		1375.22	
49	1440.61		1375.22	
50	1440.61		1375.64	
51	1452.71			
52	1459.58			
53	1458.59			
54	1464.53			
55	1464.53			
56	1473.41			
57	1473.56			
58	1473.57			
59	1473.60			
60	1473.62			
61	1481.89			
62	1496.82			
63	1496.83			
64	1498.33			
65	1498.33			
66	1500.21			
67	1506.17			
68	1506.18			
69	1506.33			
70	1506.34			
71	1506.38			
72	1513.61	T1ND4		
73	1513.62	T1ND4		
74	1518.45	T1ND4		
(Mode 75–78)				
75	1518.45	T1ND5		
76	1520.23	T1ND5		
77	1523.66	T1ND5		
78	1523.71	T1ND6		

at the right side of the figure represent the displacement values. In Fig. 12, all of the displacements are positive and that indicates all of the blades are deformed in the positive z-direction and the supported disk does not undergo any displacement. In Fig. 13, one nodal diameter is shown in this mode. It is clear that the upper left part of the model has F, G, H, and I which represent the positive displacement and the lower right part of the model has A, B, C, D, and E which represent

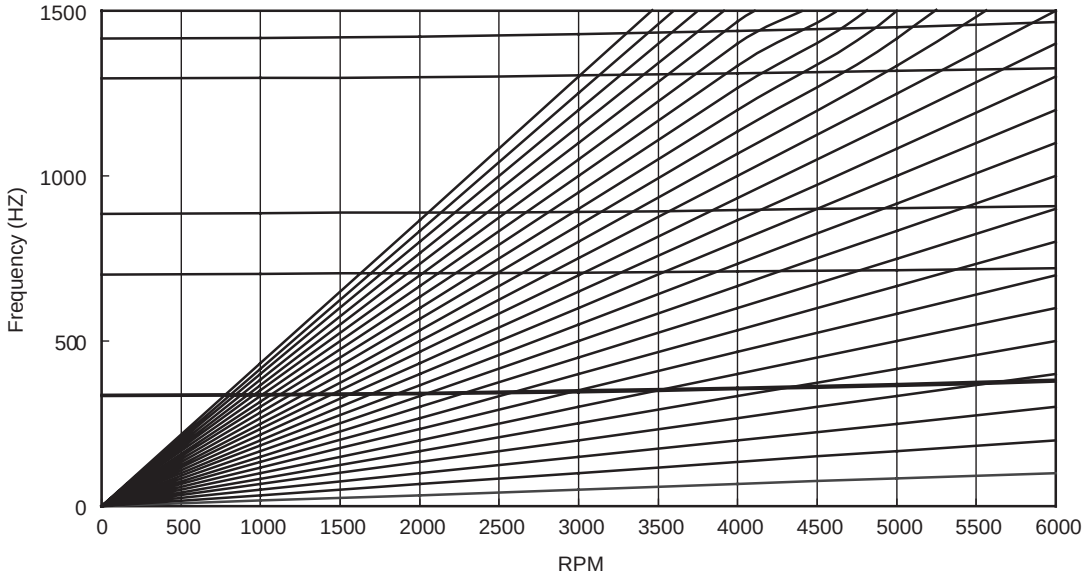

Fig. 10. The Campbell diagram of the full model of 5 groups of 12 blades.

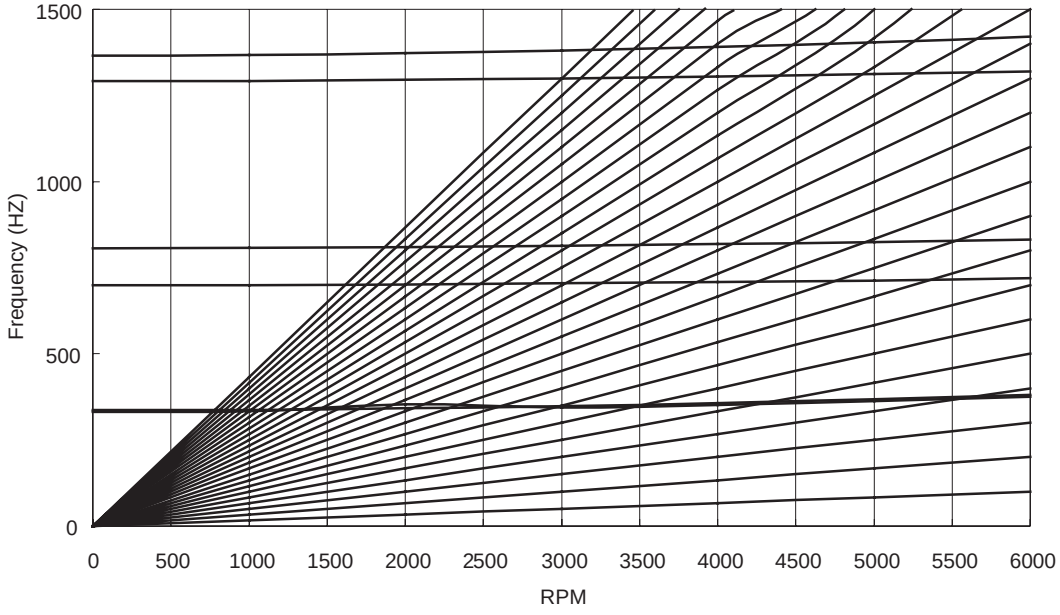

Fig. 11. The Campbell diagram of the model of 10 groups of 6 blades.

the negative displacement. Between the positive and negative displacements there exists one line that there is no displacement value. The above explanations can be used in Figs. 14–19 to understand the number of nodal diameters. Four nodal diameters are shown in Fig. 14, and three nodal diameters are plotted in Fig. 15. For comparison, the mode shape for the other blade system

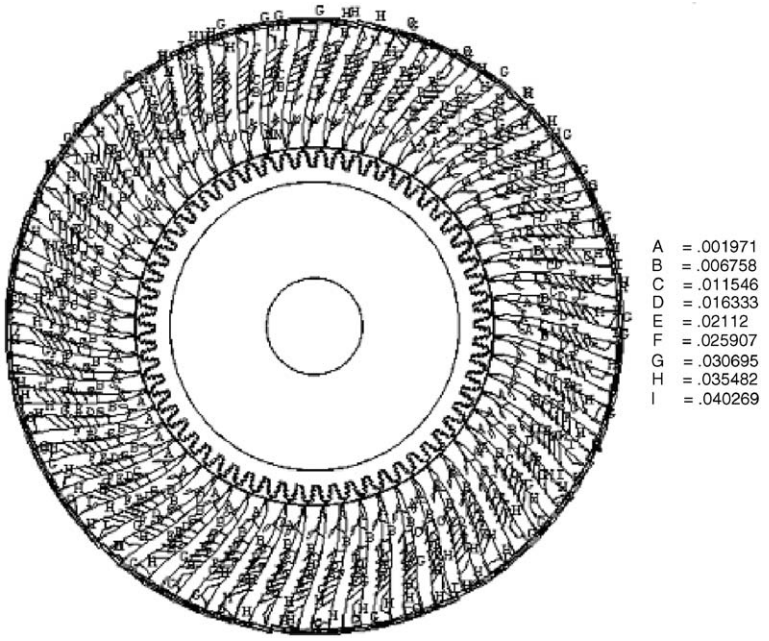

Fig. 12. The first mode of the model with 10 groups of 6 blades (Nodal diameter = 0).

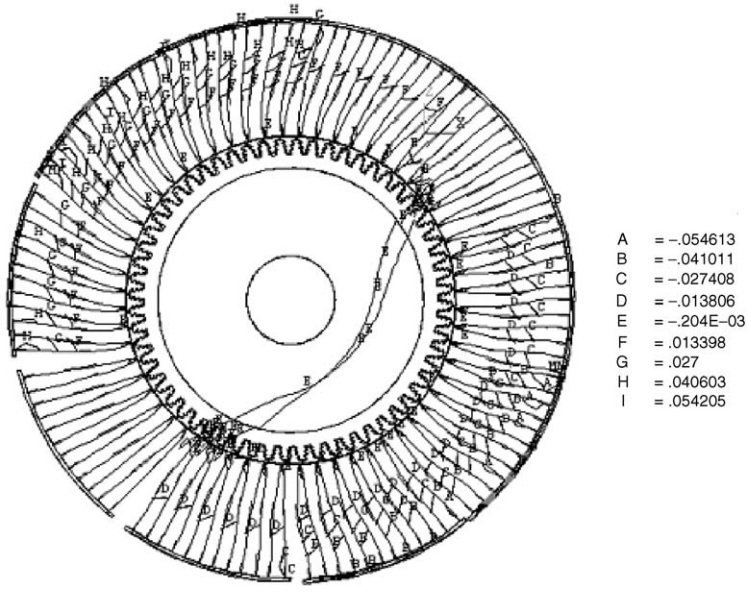

Fig. 13. The 2nd mode of the model with 10 groups of 6 blades (Nodal diameter = 1).

with 12 blades groups is shown in Figs. 16–19. In Fig. 16, no nodal diameter is shown because the concave shape is observed as in Fig. 12. Two nodal diameters are observed in Fig. 17, and 3 are observed in Figs. 18 and 19.

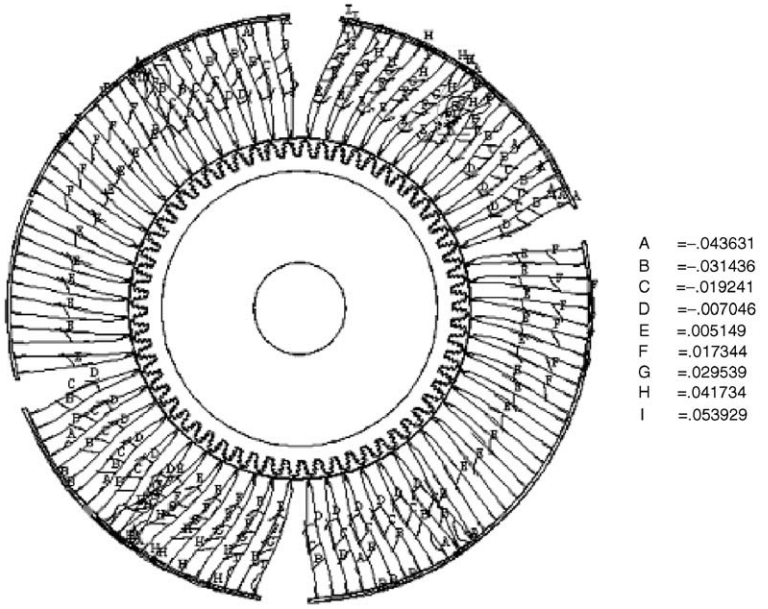

Fig. 14. The 3rd mode of the model with 10 groups of 6 blades (Nodal diameter = 4).

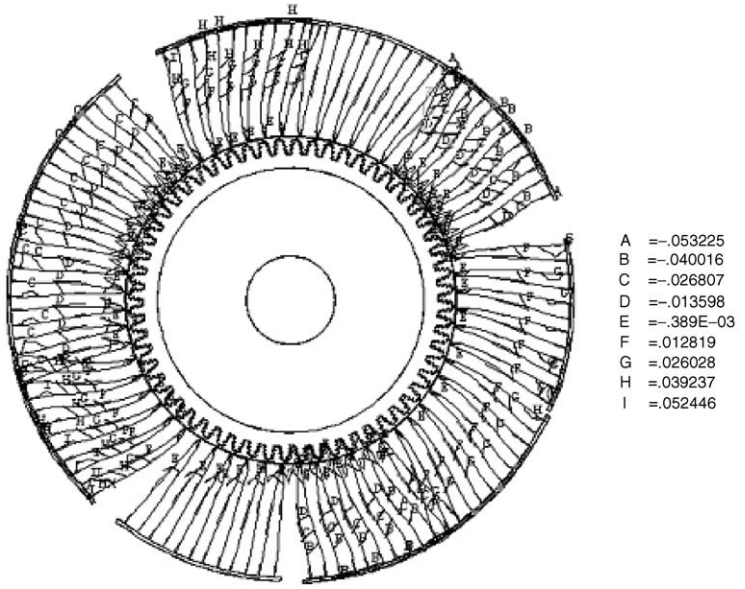

Fig. 15. The 4th mode of the model with 10 groups of 6 blades (Nodal diameter = 3).

From these eight mode shapes, we see that for the same cycle of 60 blades the grouping of blades is different, then dynamic behaviors are also significantly different. In Campbell diagram for full circle of blades with 10 groups with 6 blades in each group (see Fig. 11), one sees rotating speeds between 4000 and 4500 r.p.m., the cross-point between the natural frequency line and 5th

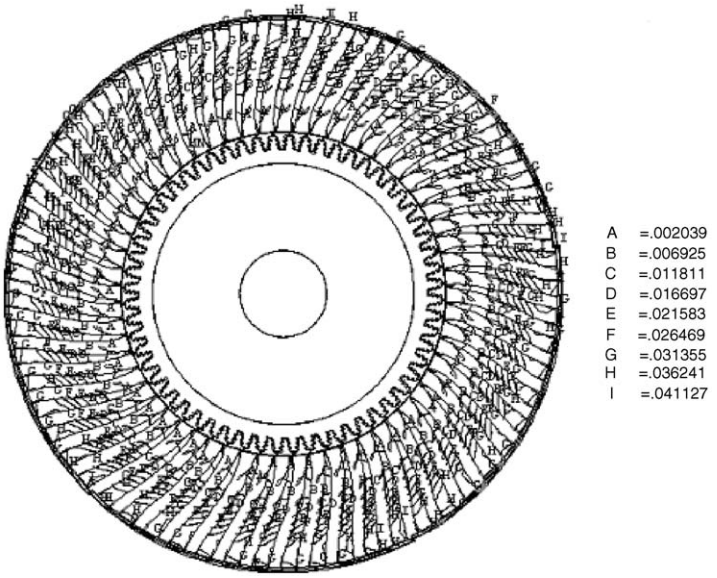

Fig. 16. The 1st mode of the model with 5 groups of 12 blades (Nodal diameter = 0).

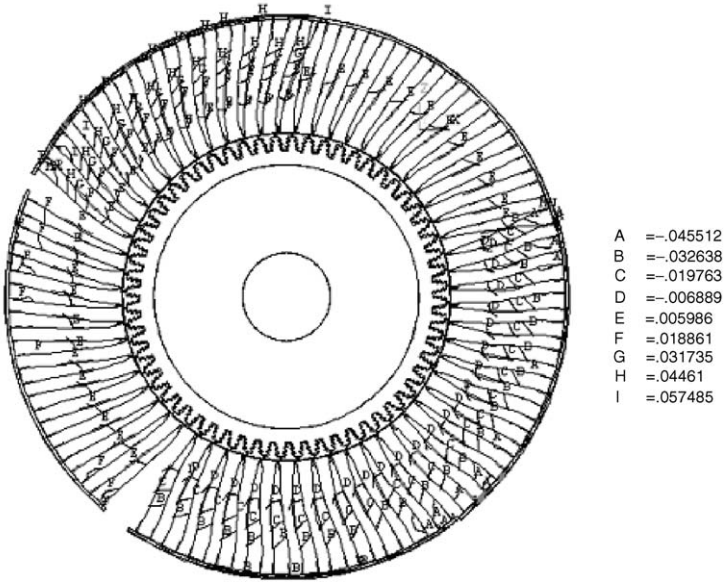

Fig. 17. The 2nd mode of the model with 5 groups of 12 blades (Nodal diameter = 2).

harmonics line. The nodal diameter of 5 in the first vibration group of the model with 10 groups of blades is also listed in Table 5. The other rotating speed around 5500 r.p.m., the cross-point between the natural frequency line corresponding to the first vibration group and the 4th harmonics line is obtained. Therein, two resonant rotating speeds appear between 4000 and 4500 r.p.m. and around 5500 r.p.m. could be obtained for the model of 10 groups of 6 blades.

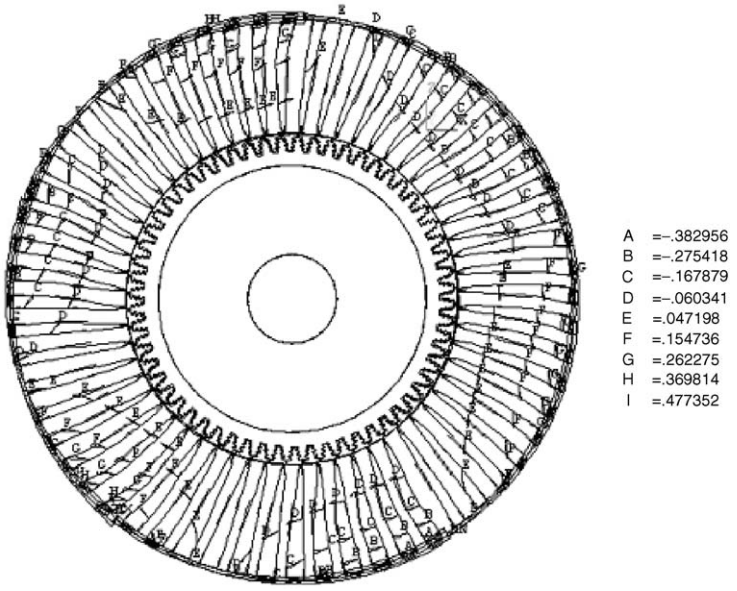

Fig. 18. The 3rd mode of the model with 5 groups of 12 blades (Nodal diameter = 3).

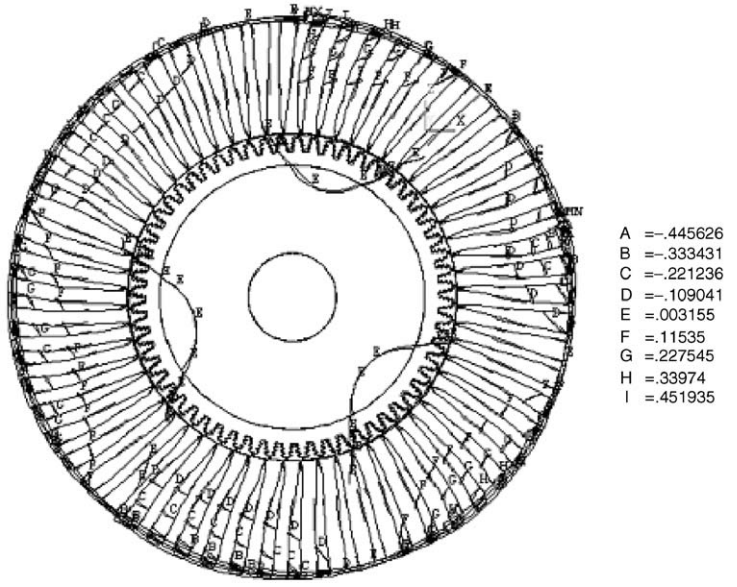

Fig. 19. The 4th mode of the model with 5 groups of 12 blades (Nodal diameter = 3).

Based on the same analytical method, the resonant rotating speed for the model of 5 groups of 12 blades could not be found from Table 5 and Fig. 7. From the Campbell diagram shown in Fig. 10, the cross-point for the first vibration group of the model with 5 groups of blades is still observed at the 4th and 5th harmonics lines, but the nodal diameter number shown in Table 5 has no 4 and 5. From these calculations, it is clear that there is no resonant rotating speed for the system with 5

groups of 10 blades in the first vibration group. It means that the resonant vibration behavior appear in the system of 10 groups of 6 blades and not in the system of 5 groups of 10 blades.

One more interesting thing found is that number of modes in the first vibration group of the system with 5 groups of 12 blades is less than that found in the system with 10 groups of 6 blades, in the higher mode listed in the mode numbers 71–77 listed in Table 5. The nodal diameters of 4 and 5 shown in the system of 10 groups of 6 blades right now are shifted to the higher mode number in the third vibration group for the system of 5 groups of 12 blades. These results pointed out that changing the blades number in a group cannot delete the original mode but shifts the lower mode to be higher mode and can avoid the resonant vibration behavior to reduce the chance of the blade failure.

Based on the above observations, we note that blade system of a group of 6 blades has opportunity to get the resonant frequencies and the group of 12 blades has no resonant phenomena in the 1st range of the frequency range. Due to the higher nth harmonics lines in the range of 2nd and 3rd vibration frequencies, a system with 5 groups of 12 blades will not have any change to get the resonant phenomena and more detailed analyses are not necessary.

6. Steady state stress analysis of systems of 10 group of 6 blades and 5 groups of 12 blades

The blades in turbine engine will be subjected to many external loads including the centrifugal force due to the rotating speed, and the surface pressure due to the flowing steam. These loads may have many interactions between the blades, blade shrouds, blade roots, and disk. The stress analyses of a circle of 60 blades are performed in this section. The governing equation used in this analysis is of a simple form: $[k]\{u\} = \{F\}$, where $[k]$ is the stiffness matrix, $\{u\}$ is the displacement vector and $\{F\}$ is the centrifugal force. $\{F\} = \vec{\mathbf{Z}} R_I \boldsymbol{\omega}^2$, where R_I is the distance between any point in the blade system and the rotating center, and ω is the rotating speed.

In this section, the surface contact elements between the blade roots and disk are generated to replace the merging nodes in the rotating vibration analysis. In Fig. 20, the contact elements for a group of 6 blades are shown and the detailed contact elements are plotted in Fig. 21. The surface contact elements for a group of 12 blades are shown in Fig. 22 and the detailed surface contact elements are plotted in Fig. 23.

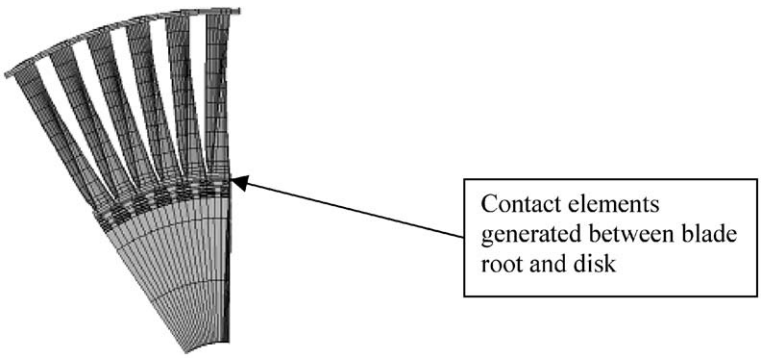

Fig. 20. Surface contact elements created between blade root and disk.

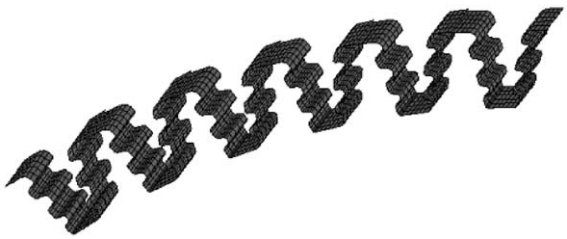

Fig. 21. Enlargement of the surface contact elements.

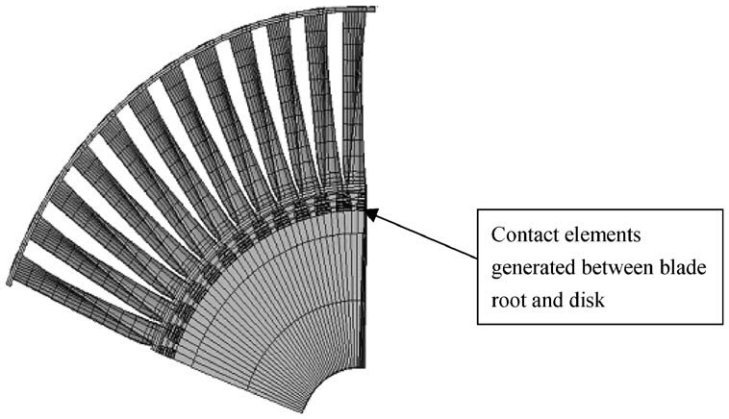

Fig. 22. Surface contact elements created between blade root and disk.

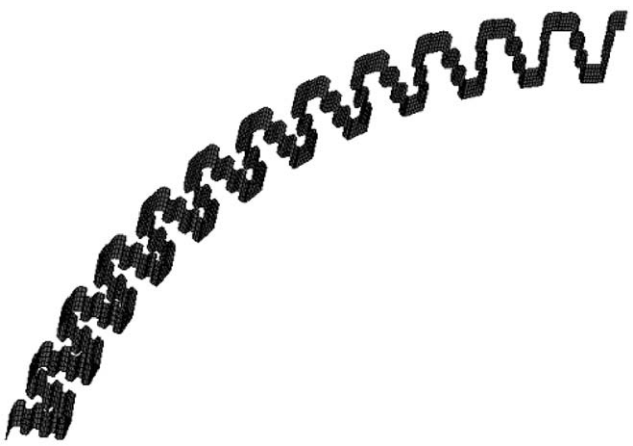

Fig. 23. Enlargement of the surface contact elements.

All these surface contact elements are only generated along the surface between the blade root and disk contact area. The surface contact elements will have the advantages that the separation or contact together of the blade root and disk during the blades are under the rotating inertia loading can be observed clearly. The maximum average stresses at the blade root are functions of

Table 6
Static rotating analysis results for a group of 6 blades (contact element)

RPM	1000	2000	3000	4000	5000	6000
DMX (mm)	0.012318	0.03871	0.094371	1.19E−01	1.84E−01	2.49E−01
σ eqv (mpa) (Ave.)	5.91	15.68	34.43	43.08	65.02	86.96

Table 7
Static rotating analysis results for a group of 12 blades (contact element)

RPM	1000	2000	3000	4000	5000	6000
DMX (mm)	0.013309	0.041824	0.10198	1.29E−01	1.99E−01	2.69E−01
σ eqv (mpa) (Ave.)	6.29	16.68	36.61	45.71	69.08	92.47

the rotating speed and are summarized in Tables 6 and 7. The steady state stresses for the system with different groups of blades are increasing as the rotating speed increases.

The rotating speeds calculated from the Campbell diagram are 4338 and 5650 r.p.m. and are expected to have the resonant vibration behavior. Two rotating speeds are obtained from different rotating speeds and multiple harmonic lines.

The stresses obtained here will be the mean stress that is described in the Goodman diagram. The alternative stress will be calculated from the next section and the harmonic analysis would be performed. Combination of the mean stresses and the alternative stresses will be used to calculate the fatigue life.

7. Harmonic analysis of a circle of 60 blades

Harmonic response analysis is a technique used to determine the steady state response of a linear structure to loads that vary sinusoidally (harmonically) with time. The idea is to calculate the structure's response at several frequencies and obtain a graph of some response (usually displacements) versus frequency, and ''peak frequencies''. For the details of the procedure, please see Ref. [37].

The harmonic force that is caused by non-uniform steam flow will apply to the blade system. The frequency of the harmonic force is a multiple of the natural frequency of the blade system. If the frequency of the harmonic force is very close or equal to the nature frequency of the blade system, the resonant vibration will be observed and large vibration amplitude of the blade system will be obtained and the fatigue life of the system will be reduced very much. The governing equation for harmonic analysis is the following:

$$[M]\{\ddot{u}\} + [C]\{\dot{u}\} + [k]\{U\} = F_n e^{i\omega t},$$

where $[M]$ is the mass matrix, $[C]$ is the damping matrix, $[k]$ is the stiffness matrix, $\{u\}$ is the displacement vector, F_n is the amplitude of the harmonic force, and ω is the rotating speed.

The exciting force is represented by sine function and is called harmonic exciting force. The stiffness matrix is not only from the structure itself, but also from the rotating speed of the structure.

The rotating speeds applied in this analysis were 4338 and 5650 r.p.m. obtained in the previous section. The forces F_n applied to the airfoil of the blade are difficult to get, when computational fluid dynamic (CFD) is applied to perform analyses and even then one may have to spend much time. In this research, a simplified method is proposed in this analysis based on pressure and temperature at inlet and outlet of turbine engine with the Mollier map of water that showed the relationship between enthalpy (h), entropy (s), temperature and pressure. For one steam turbine engine, the inlet pressure is 138 PSIG (gage pressure) and temperature is 680°F, the outlet pressure is 2.6 in HgA (A = absolute pressure) and it is equal to 1.28 psi. The atmosphere pressure is 14.7 psi, and hence, the inlet pressure will be 138 psi + 14.7 psi = 152.7 psi.

Combining all these data with the Mollier map one gets a pressure of 1.8 psi at pressure side and 1.277 psi at suction side of the blades. The damping ratio is 0.2% and it is the average values from the modal tests. The mode superposition method is selected to perform the harmonic analysis. Due to the high stress appearing near node 225, the harmonic responses are plotted at this node number. The frequency response at node number of 225 is shown in Fig. 24 for the rotating speed 5650 r.p.m. and in Fig. 25 for the rotating speed 4338 r.p.m.

From both of these results, the resonant frequency is around 360 Hz. The exact resonant frequency ith a rotating speed of 5650 r.p.m. is 376.8 Hz. The stress distributions for these resonant conditions that corresponding to the rotating speed of 5650 r.p.m. are plotted in Fig. 26 and that corresponding to the rotating speed of 4338 r.p.m. in Fig. 27. Also the location of peak stresses is at the location of initial crack. This initial crack location results in the failure of the blade. The location of the peak stresses found here is exactly in the location shown in Fig. 1 in which the in-site picture of the blade failure is provided.

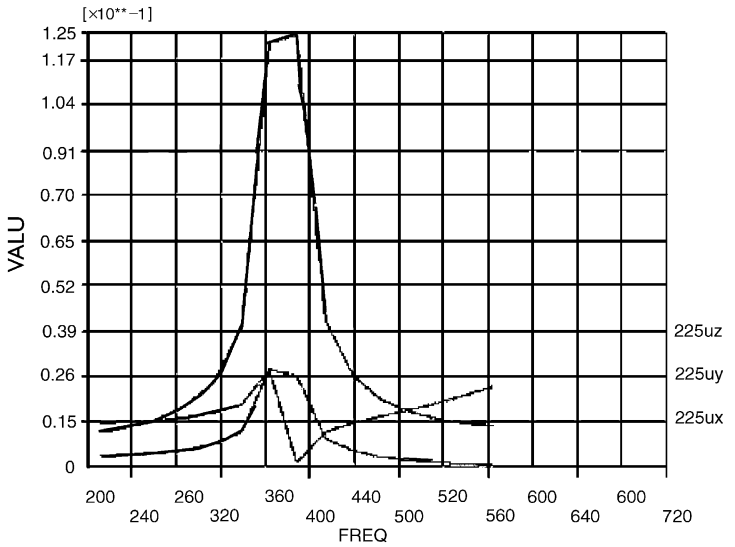

Fig. 24. The frequency response at node 225 for model with 10 groups of 6 blades (r.p.m. = 5650).

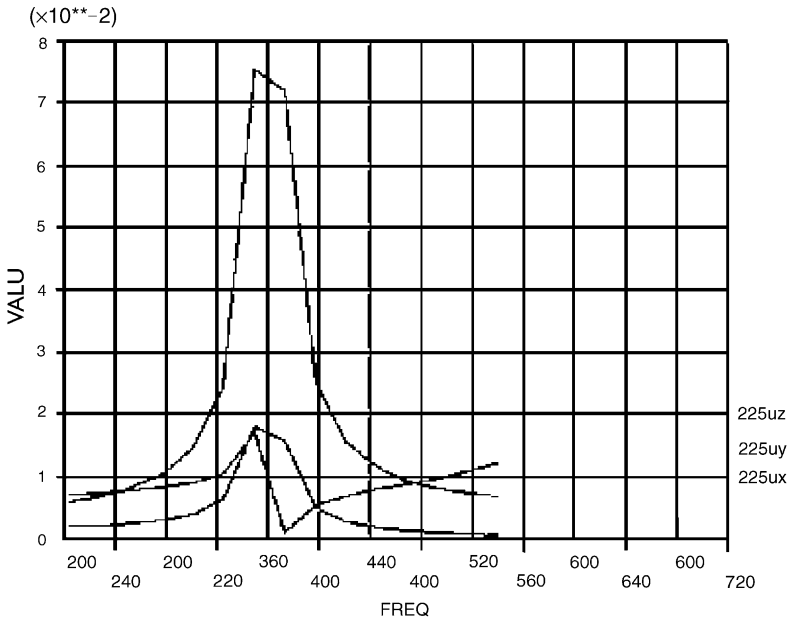

Fig. 25. The frequency response at node 225 for model with 10 groups of 6 blades (r.p.m. = 4338).

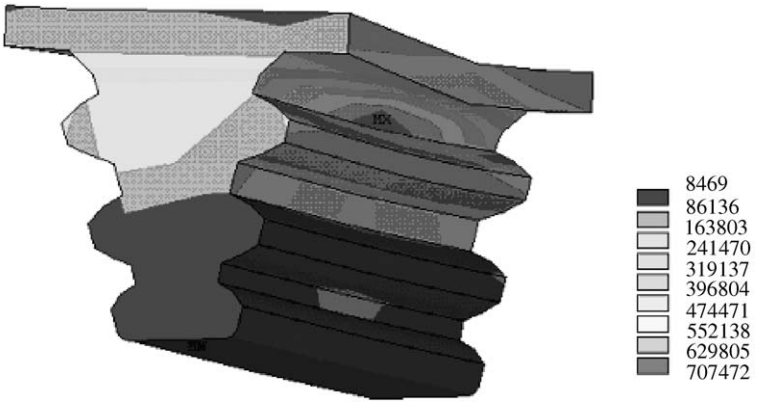

Fig. 26. Stress distribution of the blade root from the harmonic analysis (r.p.m. = 5650).

8. Conclusions

The free–free vibration of a single blade from the finite element analytical results can match very well with the experimental data. The natural frequency of a single blade obtained from FEM is only within 5% difference compared with the test results. The mode shapes from FEM agree completely with the results observed in the experimental results. Therefore, the finite element method is confirmed by the experimental tests to be a good method for performing dynamic analysis of complicated geometric blades.

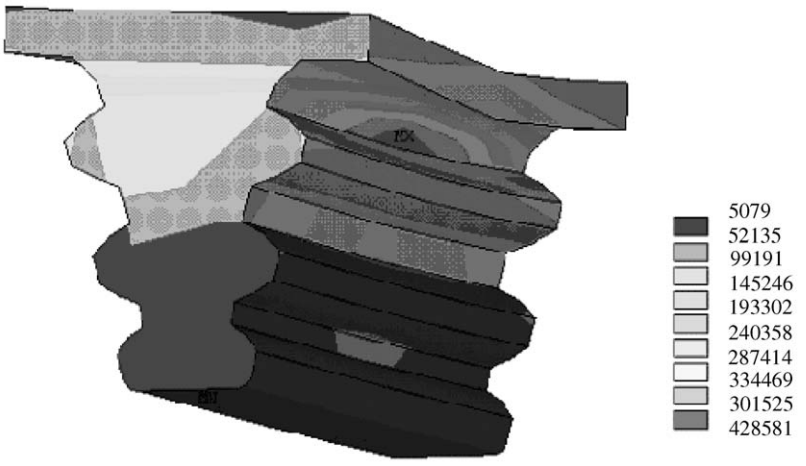

Fig. 27. Stress distribution of the blade root from the harmonic analysis (r.p.m. = 4338).

The Campbell diagram obtained from circles of 60 blades but having different number of groups can be used to calculate their resonant rotating speed. Combination of the Campbell diagram and mode shapes for the model with 5 groups of 10 blades are not found in the first vibration group. The model with 10 groups of 6 blades resonant rotating speeds of 4338 and 5650 r.p.m. and their corresponding stresses are also obtained through the harmonic analysis. The location of the maximum stresses is observed from the FEM and is completely matched with the observation from in-site field as shown in Fig. 1.

The other interesting conclusion is that the nodal diameters 4 and 5 observed in the first vibration group of the model with 10 groups of 6 blades are not observed in the same vibration range of the model with 5 groups of 12 blades. Although all of these mode shapes for nodal diameters of 4 and 5 for the model with 5 groups of 12 blades do not appear in the first vibration group, they can be observed in the higher mode numbers such as 71–77 that belong to the higher mode of the third vibration group. Therein, the mode shapes of the higher nodal diameter in the first vibration group in the model with 10 groups of blades shifts to the third vibration group of the model with 5 groups of 12 blades. And this shift has a significant effect in that the resonant rotating speed disappears in the model with 5 groups of 12 blades but is found in the model with 10 groups of 6 blades. This means that a circle of 60 blades with 5 groups of 12 blades can avoid resonant vibration and extend their fatigue life.

References

[1] S.P. Timoshenko, Vibration Problems in Engineering, Van Nostrand, Princeton, NJ, 1955.
[2] S.P. Timoshenko, J.N. Goodier, Theory of Elasticity, McGraw-Hill, New York, 1961.
[3] J.S. Rao, J.H. Wang, Lecture Notes on Rotor Dynamics, Unsteady Blade Loading, Blade Heat Transfer and Blade Vibration of Turbomachines, Part II, Head Office of Taiwan Power Company, Taipei, Taiwan, ROC, August 1995.

[4] N.O. Myklestad, New method of calculating natural modes of uncoupled bending vibration, Journal of Aerosol Science 48 (1944) 153.
[5] M.A. Prohl, A general method of calculating critical speeds of flexible rotors, Journal of Applied Mechanics, American Society of Mechanical Engineers 12 (1945) A–142.
[6] B. Downs, Vibration analysis of turbomachinery blades using dedicated discretization and twisted beam theory, ASME, 79-DET-85.
[7] W. Carnegie, J. Thomas, The coupled bending-bending vibration of pre-twisted tapered blading, Journal of Engineering for Industry Transactions, American Society of Mechanical Engineers 94 (1972) 255.
[8] W. Carnegie, J. Thomas, The effect of shear deformation and rotary inertia on the lateral frequencies of cantilever beams in bending, Journal of Engineering for Industry Transactions, American Society of Mechanical Engineers 94 (1972) 267.
[9] O.C. Zienkiewicz, The Finite Element Method in Engineering Science, McGraw-Hill, London, 1971.
[10] E. Dokumaci, Development and Application of the Finite Element Method to the Vibration Of Beams, Ph.D. Thesis, University of Surrey, England, 1968.
[11] W. Carnegie, J. Thomas, E. Dokumaci, An improved method of matrix displacement analysis in vibration problems, Aeronautical Quarterly 20 (1969) 321.
[12] A.V.K. Murthy, S.S. Murthy, Finite element analysis of rotor, Mechanism and Machine Theory 12 (4) (1977) 311.
[13] R.S. Gupta, S.S. Rao, Finite element eigen value analysis of tapered and twisted Timoshenko beams, Journal of Sound and Vibration 56 (2) (1978) 187.
[14] B.A.H. Abbas, Simple finite elements for dynamic analysis of thick pre-twisted blades, Aeronautical Journal 83 (827) (1979) 450.
[15] S. Putter, H. Manor, Natural frequencies of radial rotating beams, Journal of Sound and Vibration 56 (2) (1978) 175.
[16] V.K. Singh, S. Rawtani, The effect of root flexibility on torsional vibration of uniform section blades, International Journal Mechanical Science 21 (3) (1979) 141.
[17] V.T. Nagaraj, N. Sabu, Torsional vibrations of non-uniform rotating blades with attachment flexibility, Journal of Sound and Vibration 80 (3) (1982) 401.
[18] N.F. Rieger, W.J. Nowak, Analysis of Fatigue Stresses in Steam Turbine Blade Groups, EPRI seminar on Steam Turbine Availability, Palo Alto, CA, January 1977.
[19] J. Thomas, H.T. Belek, Free vibrations of blade packets, Journal of Mechanical Engineering Science 19 (1) (1977) 13.
[20] A.L. Salama, M. Petyt, Dynamic response of packets of blades by the finite element method, Journal of Mechanical Design Transactions, American Society of Mechanical Engineers 100 (4) (1978) 660.
[21] F.E. Sagendorph, Natural frequencies of mid-span shrouded fan blades, presented at ASME Vibration Conference, 1977.
[22] H.M. Lee, G.C. Foile, L.B. Perkins, Finite Element Analysis of the Space Shuttle Main Engine (SSME) High Pressure Full Turbo Pump Turbine Blade (HPEIP), Marshall Space Flight Center letter EHZE 137-28, Huntsville, Albama, Harch, 1987.
[23] A. Bazoune, Y.A. Khulife, A finite element for vibration analysis of rotating tapered Timoshenko beams, Journal of Sound and Vibration 156 (1) (1992) 141–164.
[24] V. Omparkash, T.C.T. Lam, D. Gruwell, T.H. McCloskey, Life extension strategies of cracked disk attachment for the power generation Industry, American Society of Mechanical Engineers (1994) 139–164.
[25] O. Rand, Free vibration of thin-walled composite blades, Composite Structures 28 (1994) 169–180.
[26] T.N. Shiau, Y.D. Yu, E.P. Kuo, Vibration and optimum design of rotating laminated blades, Composites Part B 27 (1996) 173–183.
[27] K.M. Liew, C.W. Lim, A global continuum Ritz formulation for flexural vibration of pretwisted trapezoidal plates with one edge built in, Computer Methods in Applied Mechanics and Engineering 114 (1994) 233–247.
[28] K.M. Liew, M.K. Lim, C.W. Lim, D.B. Li, Y.R. Zhang, Effects of initial twist and thickness variation on the vibration behaviour of shallow conical shells, Journal of Sound and Vibration 180 (2) (1995) 271–296.
[29] C.W. Lim, K.M. Liew, Vibration of pretwisted cantilever trapezoidal symmetric laminate, Acta Mechanica 111 (1995) 193–208.

[30] K.M. Liew, C.W. Lim, Vibratory characteristics of pretwisted cantilever trapezoids of unsymmetric laminates, American Institute of Aeronautics and Astronautics Journal 34 (5) (1996) 1041–1050.
[31] C.W. Lim, K.M. Liew, S. Kitipornchai, Free vibration of pretwisted, cantilevered composite shallow conical shells, American Institute of Aeronautics and Astronautics Journal 35 (2) (1997) 327–333.
[32] H.T. Lin, J.J. Lin, Nonlinear hydro elastic behavior of propellers using a finite-element method and lifting surface theory, Journal of Marine Science and Technology 1 (1996) 114–124.
[33] R. Bladh, M.P. Castanier, C. Pieer, Reduced order modeling and vibration analysis of mistuned blade disk assemblies with shrouds, Journal of Engineering for Gas Turbines and Power 121 (1999) 515–522.
[34] K.J. Bathe, S. Bolourchi, A geometrical and material nonlinear plate and shell element, Computers and Structures 11 (1980) 23–48.
[35] W.E. Haisler, J.A. Stricklin, Development and evaluation q solution procedures for geometrically nonlinear structural analysis, Journal of American Institute of Aeronautics and Astronautics 10 (1972) 264–272.
[36] S. Sreenivasa marshy, V. Ramamurti, A parametric study of vibration of rotating pre-twisted and tapered low aspect ratio cantilever plates, Journal of Sound and Vibration 76 (1981) 311–328.
[37] ANSYS 6.1 User's Manual, ANSYS Inc., Canonsburg, PA, 2002.